The chaperone dynein LL1 mediates cytoplasmic transport of empty and mature hepatitis B virus capsids

Quentin Osseman, Lara Gallucci, Shelly Au, Christian Cazenave, Elodie Berdance, Marie-Lise Blondot, Aurelia Cassany, Dominique Bégu, Jessica Ragues, Cindy Aknin, et al.

The chaperone dynein LL1 mediates cytoplasmic transport of empty and mature hepatitis B virus capsids

Quentin Osseman[1,2,y], Lara Gallucci[1,2], Shelly Au[3,‡], Christian Cazenave[1,2], Elodie Berdance[1,2], Marie-Lise Blondot[1,2], Aurélia Cassany[1,2], Dominique Bégu[1,2], Jessica Ragues[1,2], Cindy Aknin[1,2], Irina Sominskaya[4], Andris Dishlers[4], Birgit Rabe[5,§], Fenja Anderson[5,6], Nelly Panté[3], Michael Kann[1,2,5,7,⇑]

[1]*Univ. de Bordeaux, Microbiologie Fondamentale et Pathogénicité, UMR 5234, 33076 Bordeaux, France;* [2]*CNRS, Microbiologie Fondamentale et Pathogénicité, UMR 5234, Bordeaux, France;* [3]*Department of Zoology, University of British Columbia Vancouver, B.C. V6T 1Z4, Canada;* [4]*Latvian Biomedical Research and Study Center, 1067 Riga, Latvia;* [5]*Institute of Medical Virology, University of Giessen, 35392 Giessen, Germany;* [6]*Institute of Virology, Hannover Medical School, 30625 Hannover, Germany;* [7]*CHU de Bordeaux, 33000 Bordeaux, France*

Background & Aims: Hepatitis B virus (HBV) has a DNA genome but replicates within the nucleus by reverse transcription of an RNA pregenome, which is converted to DNA in cytoplasmic capsids. Capsids in this compartment are correlated with inflammation and epitopes of the capsid protein core (Cp) are a major target for T cell-mediated immune responses. We investigated the mechanism of cytoplasmic capsid transport, which is important for infection but also for cytosolic capsid removal.

Methods: We used virion-derived capsids containing mature rcDNA (matC) and empty capsids (empC). RNA-containing capsids (rnaC) were used as a control. The investigations comprised pull-down assays for identification of cellular interaction partners, immune fluorescence microscopy for their colocalization and electron microscopy after microinjection to determine their biological significance.

Results: matC and empC underwent active transport through the cytoplasm towards the nucleus, while rnaC was poorly transported. We identified the dynein light chain LL1 as a functional interaction partner linking capsids to the dynein motor complex and showed that there is no compensatory transport pathway. Using capsid and dynein LL1 mutants we characterized the required domains on the capsid and LL1.

Conclusions: This is the first investigation on the detailed molecular mechanism of how matC pass the cytoplasm upon infection and how empC can be actively removed from the cytoplasm into the nucleus. Considering that hepatocytes with cytoplasmic capsids are better recognized by the T cells, we hypothesize that targeting capsid DynLL1-interaction will not only block HBV infection but also stimulate elimination of infected cells.

Lay summary: In this study, we identified the molecular details of HBV translocation through the cytoplasm. Our evidence offers a new drug target which could not only inhibit infection but also stimulate immune clearance of HBV infected cells.

Introduction

Hepatitis B virus (HBV) infection is a global health burden causing 800,000 deaths per year,[1] resulting from chronic infections. HBV is an enveloped pararetrovirus needing the nuclear transcription machinery for multiplication.[2] The virion contains a capsid of 36 nm, which is composed of 240 copies of core protein (Cp). It comprises the relaxed circular (rc) viral DNA genome (rcDNA), the viral polymerase (pol) and heat shock proteins. HBV enters cells by receptor-mediated endocytosis,[3,4] leading to release of the capsid and retrograde cytosolic capsid transport to the nucleus,[5] subsequent passage through nuclear pore complexes (NPCs) into the nuclear basket, followed by rcDNA release.[6,7] The rcDNA is repaired to a covalently closed circular DNA (cccDNA), involving tyrosyl-DNA-phosphodiesterase 2 (TDP2)[8] and DNA polymerase j (POLK).[9] cccDNA is the matrix for transcription of the viral mRNAs[10] including the RNA, which is the template for Cp and pol translation. Pol binds to the pregenome, allowing its interaction with Cp, leading to assembly of RNA-containing capsids (rnaC). Genome maturation inside the capsid comprises reverse transcription and incomplete second strand DNA synthesis.[11] Capsids containing rcDNA (matC) form progeny HBV, while rnaC fail to interact with the viral surface proteins *in cellulo*,[12] although pregenome-containing HBV were found in some patients.[13]

Infected hepatocytes contain rnaC, capsids with maturation intermediates, few matC, and – as Cp are overexpressed – empty capsids (empC). empC also interact with the surface proteins,[14] suggesting a similar structure to matC, which differs from that of rnaC. However, while empC interact with the nuclear import

receptor importin-b directly,[16] matC need the adaptor molecule importin-a demonstrating differences in exposure of the C terminus of Cp (carboxyterminal domain [CTD]) to which both importins bind.[5,15] Such CTD exposure could also be observed in rnaC, but only after CTD phosphorylation (PrnaC).[16]

Chronicity of hepatitis B is caused by an insufficient MHC class I-mediated CD8+ T cell response directed against viral epitopes on the surface of infected hepatocytes.[17] These epitopes are predominantly derived from proteasomal degradation of Cp,[18] which then proceed via transporter associated with antigen processing to the plasma membrane. Consistently, cytosolic capsids are associated with liver inflammation in infected patients.[19,20]

Current treatment is based on nucleos(t)ides analogues suppressing genome maturation without affecting the very stable cccDNA,[21] requiring continuous inhibitor application. An alternative is PEG interferon a2b, which stably reduces viral load in one-third of patients.[22] These limitations ask for further treatment options and several clinical trials are ongoing including inhibitors of pol, HBV entry and secretion, capsid assembly inhibitors or immune modulators.[23]

While immune modulators may lead to excessive cell death, directly acting molecules neither eliminate cccDNA nor infected hepatocytes. However, their clearance might be stimulated by increasing the amount of cytoplasmic Cp, which are physiologically moved into the nucleus or removed by secretion. Of particular interest are empC as they are less stable than immature capsids and matC[24] and their degradation could increase core epitope exposure.

Hepatocytes in infected livers exhibit numerous empty nuclear capsids, indicating that nuclear transport is a major cellular pathway for cytoplasmic capsid removal. However, the high viscosity of the cytoplasm makes diffusion of larger structures inefficient[25,26] requiring active translocation which is mainly facilitated by microtubules (MTs) and which is highly conserved from algae to man.[27]

MTs allow directed transport by tubulin polymerization or depolymerization as it occurs *e.g.* during chromosome segregation.[28] With a velocity of approximately 25 nm/s[29] this transport is slow and is mediated by direct cargo tubulin-interaction. The majority of cargos use molecular motors for cytoplasmic transport. Retrograde transport is facilitated by cytosolic dynein 1, which is composed of 12 to 14 chains (Fig. S1). Two identical dynein heavy chains (DynHCs) move the complex along the MT with a velocity of up to 1,000 nm/s.[30] DynHCs are bound to two dynein light intermediate chains (DynLICs) and two dynein intermediate chains (DynICs).[31] The two DynICs are held together by a homodimer of DynLC8 – termed dynein light chain LC8-type 1 or 2 (DynLL1 and DynLL2) in vertebrates – which form a groove through which DynIC pass. DynIC dimerization is further stabilized by the light chain, DynLC7 – named roadblock 1 and 2 (DynLRb1 and DynLRb2) in vertebrates – and homodimers of dynein light chain Tctex-type 1 or 3 (DynTctex 1 [DynLT1] and DynTctex 3 [DynLT3]). While most of the dynein chains exist only in association with the dynein motor complex, a significant part of DynLL1 is not associated with cytoplasmic dynein,[32] but acts as a chaperone supporting dimerization, which is mediated by interaction with the same groove to which the DynIC binds.

Consistent with the chaperone function, numerous DynLL1 interaction partners have been described,[33] but only interaction with 'deleted in azoospermia' (Dazl), which is required for mRNA localization in mammalian male germ cell development, was proven to be DynLC8-dependent.[34]

Material and methods

Glutathione S-transferase protein production and purification

The dynein light chains, their mutants and DynIC were expressed as glutathione S-transferase (GST)-fusion proteins in *E. coli*. Following bacterial lysis, the fusion proteins were purified using glutathione Sepharose® according to the vendor. In some assays, the GST portion of GST-DynLL1 was cleaved by factor Xa and removed. Detailed protocols on mutagenesis, protein expression, purification and cleavage are given in the supplementary information.

Capsid preparation

The supernatant of HBV-expressing HepG2.2.15 cells was used to prepare matC. After stripping off the surface proteins by NP-40 and purification,[6] the capsids were characterized for capsid-enclosed viral DNA by PCR and by Southern blot. Surface protein removal was verified by immune precipitations. rnaC was obtained by Cp expression in *E. coli* as described previously.[35] These capsids exhibit the same structure as capsids containing the RNA pregenome with the exception that the polymerase is absent (resolution limit: 10–11 Å (symmetrized) and 16–17 Å (asymmetric)[36]). empC was derived from rnaC by nuclease digestion after dissociation followed by re-association. Detailed protocols including capsid characterizations are given in the supplementary information.

Capsid – Dynein light chain interactions

A total of 0.5–2 lg of capsids was incubated with 2.5 lg of purified proteins or 1 ll rabbit reticulocyte lysate (RRL), approximately 100 lg protein, prior to sedimentation through a 60% sucrose cushion. The sediment was analyzed for capsids by native agarose gel electrophoresis (NAGE) and Western blot; GST-fusion proteins were detected by Western blot after SDS PAGE. Pull-down assays were performed using biomagnetic- or glutathione Sepharose beads followed by Western blot for detection of co-precipitated proteins. Details are described in the supplementary information.

Capsid binding to *in vitro* polymerized microtubules

Unlabeled and rhodamine-labeled tubulin was *in vitro* polymerized on glass coverslips prior to incubation with 100 ng of capsids in the presence or absence of RRL. Following 90 min incubation at RT and washing, the capsids were detected by indirect immune fluorescence. A detailed description is given in the supplementary information.

Microinjection and preparation of Xenopus laevis oocytes for EM

Defolliculated *Xenopus laevis* state VI oocytes were microinjected with 50 nl of capsids (5×10^8 empC and rnaC, 9×10^7 matC and PrnaC). The injection site was indicated by co-injection of 1% bromophenol blue. In competition experiments GST-DynLL1 or the H41Y mutant were co-injected in eightfold excess with regard to one core protein dimer. After incubation at RT, oocytes were fixed, manually dissected, and embedded in low melting agarose. After incubation with 1% OsO_4, the samples were dehydrated, Epon™-embedded, and cut into 50 nm

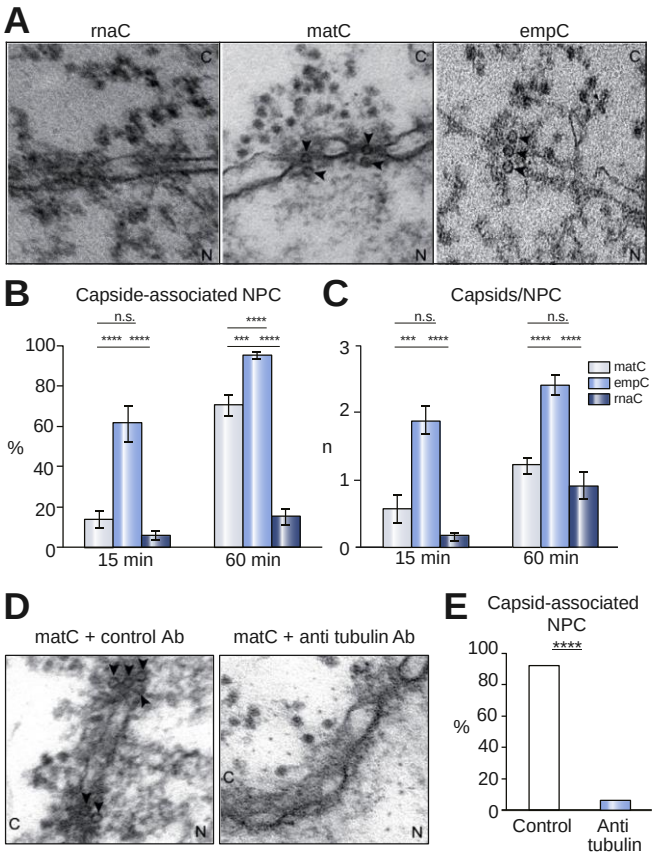

Fig. 1. Transmission electron microscopy of rnaC, matC and empC at the nuclear envelope after cytosolic microinjection into *Xenopus laevis* oocytes. (A) Electron micrographs of thin sections 60 min after microinjection. Capsids are indicated by arrows. N: nucleus, C: cytoplasm. (B) Percentage of capsid-decorated NPCs at 15 and 60 min post injection. Quantification was done on 126 sections derived from different sites of the NE of 14 microinjected oocytes. Analysis was based on 77 NPCs (15 min) and 106 NPCs (60 min) for empC, 99 NPCs (15 min) and 148 NPCs (60 min) for matC, and 113 NPCs (15 min) and 87 NPCs (60 min) for rnaC. Bars: 95% confidence intervals; *: significance by unpaired Student's *t* test with unequal variances. (C) As in B, but showing the average number of capsids per capsid-associated NPC. (D) As in A, but after pre-injection of anti-tubulin antibodies (left) or an unrelated control antibody (right) 30 min before capsid injection. (E) Percentage of empC-associated NPCs, based on 88 and 57 NPCs (control antibody, white; anti-tubulin antibody, black) two hours post microinjection. empC, empty capsids; matC, mature rcDNA; NE, nuclear envelope; NPC, nuclear pore complex; rnaC, RNA-containing capsids.

thin sections. Following negative stain on EM copper grids with 2% $C_4H_8O_6U$ and 2% $C_{12}H_{10}O_{14}Pb_3$, the samples were analyzed by transmission electron microscopy (TEM) or tomography.

For further details regarding the methods used, please refer to the CTAT table and supplementary information.

Results

Retrograde transport of capsids to the NPCs

Having characterized the capsid species (supplementary results, Fig. S2) we microinjected rnaC, empC, matC and a rnaC mutant, devoid of the CTD (ΔCC; aa 1–149, devoid of encapsidated RNA) into the cytoplasm of *Xenopus laevis* oocytes at sites approximately 400–500 µm from the nucleus. We used these cells as their large size allows much better discrimination between active transport and diffusion. Investigating capsid arrival at the nucleus 15 and 60 min post injection by TEM, we observed that both matC and empC localized on the cytoplasmic and nuclear side of the NPCs (Fig. 1A). Electron tomography verified their localization and showed that thin section images result in underestimation of the number of capsids per NPC by approximately threefold (supplementary Video 1). Few rnaC were found at the NPCs (Fig. 1A) and ΔCC were never observed at the nucleus. Considering the time and distance, these results suggest that at least empC and matC move by active retrograde transport.

To compare the efficiency of capsid displacement towards the nucleus, we quantified the number of NPC-associated capsids. We analyzed sections from different areas of the nuclear envelope (NE) to avoid quantification close to the microtubule-organizing center (MTOC) where capsids could have been more frequent. The percentage of capsid-decorated NPCs increased over time from 15% to 70% for matC and from 61% to 95% for empC (Fig. 1B). The higher percentage of empC-associated NPCs corresponds to the higher number of microinjected capsids. With 5% of rnaC-associated NPCs after 15 min, rnaC translocation was less efficient but the increase to 14% at 60 min indicated some transport.

Quantification of the average number of capsids per capsid-associated NPC showed little increase throughout the observation period (matC: 0.6 to 1.2, empC: 1.9 to 2.4, rnaC: 0.1 to 0.9) (Fig. 1C), but in contrast to empC and matC, rnaC was never observed on the nuclear NPC side. Thus, we conclude that empC and matC exhibited a similar if not identical retrograde cytoplasmic transport capacity, while rnaC was less efficiently translocated to and through NPCs.

Next, we investigated whether this transport required MTs, by injecting an excess of anti-αtubulin antibodies or an anti-parvovirus H1 control antibody 30 min prior to capsid injection (Fig. 1D). Quantification revealed that anti-αtubulin antibody pre-injection reduced the percentage of capsid-associated NPCs to 7%compared to 93%in the control (Fig. 1E).

Capsid binding to *in vitro* polymerized MT

To analyze the capsid MT-interaction in more detail, we investigated the binding of matC, empC and rnaC to *in vitro*-polymerized rhodamine-labeled MTs in the absence or presence of cytosolic factors (Fig. 2A, B). We used RRL, as such a high protein concentration can hardly be yielded by in house cell lysates. We observed that capsid binding occurred throughout the entire MT length and was strongly enhanced by adapters (Fig. 2A, B, C), but much stronger for matC and empC (matC: 7.2-fold; empC: 8.1-fold; rnaC: 1.9-fold). Further, empC- and matC-binding was significantly stronger than that of rnaC (Fig. 2D).

In vitro interaction of the capsids with dynein light chains

The linker-dependent MT binding made dynein-mediated MT transport likely. To identify potential binding partner(s), we expressed the six different dynein light chains fused to GST (Fig. S3A). Functionality was verified by pull-down assays of the DynIC from RRL (Fig. S3B).

We investigated the light chain fusion proteins for interaction with the capsids using pull-down assays and co-sedimentation through 60% sucrose cushions. Co-sedimentation has the advantage that the native complex can be analyzed without the need for a solid phase attachment site. However, it has the disadvantage that the results are more qual-

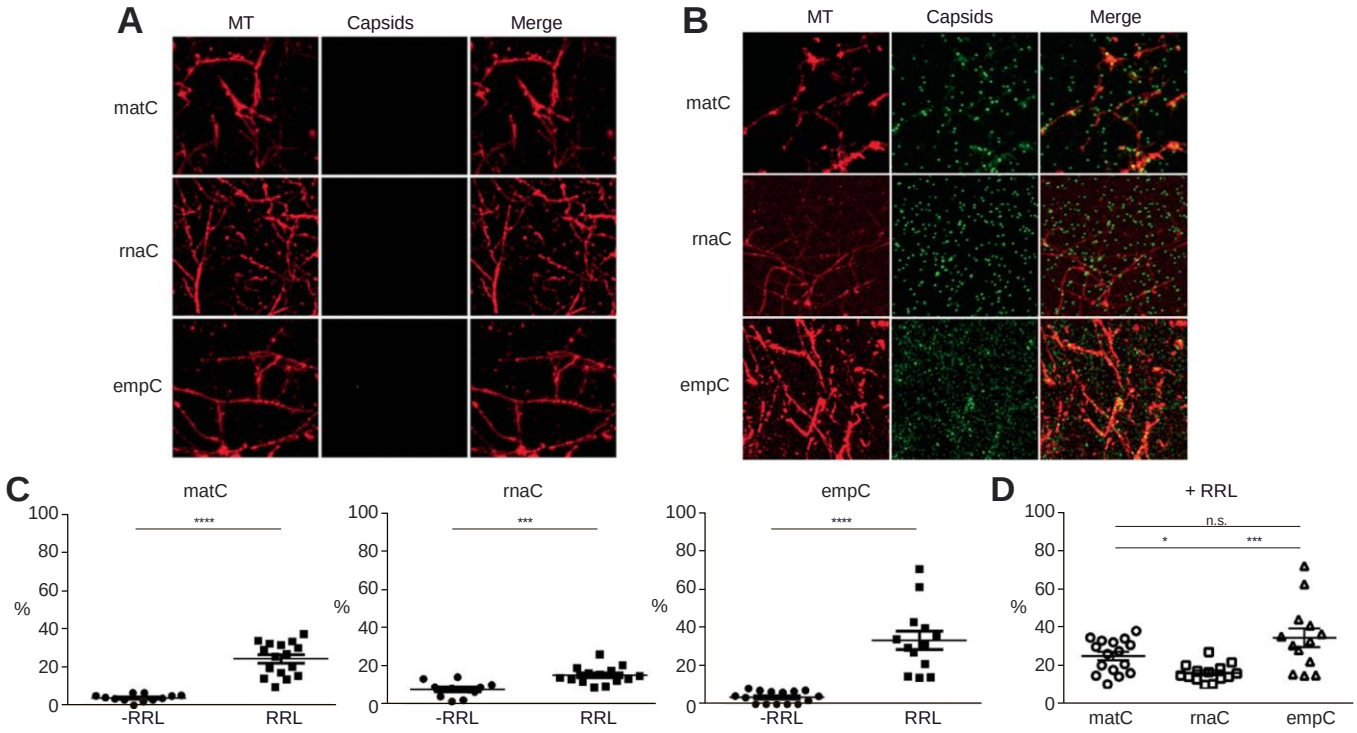

Fig. 2. *In vitro* binding of matC and empC to microtubules. (A, B) Fluorescence microscopy of *in vitro* polymerized rhodamine-labeled MT (red) and capsids (green), detected by indirect immune fluorescence. (A) In the absence of cytosolic proteins. (B) In the presence of cytosolic proteins (RRL). (C, D) Quantification of capsid MT-association. Y-axis: percentage of capsid colocalizing with MTs. Each point depicts the result for one microscopical field. Significant differences by unpaired Student's *t* Test with unequal variances are indicated by * (C) Effect of RRL on capsid binding. The capsid species is indicated on top of the panels. (D) Binding of the different capsid species in the presence of RRL. empC, empty capsids; matC, mature rcDNA; MT, microtubules; rnaC, RNA-containing capsids; RRL, rabbit reticulocyte lysate. (This figure appears in colour on the web.)

itative than quantitative because of technical limitations arising from small volumes (130 µl gradients). empC co-sedimented with GST-DynLL1 and GST-DynRb2 (Fig. 3A left panels), but DynRb2-sedimentation was capsid-independent, indicating aggregation of GST-DynRb2 (Fig. 3A right panels). empC, derived from *in vitro* disassembly and re-association after Cp purification, also co-sedimented with GST-DynLL1, excluding the possibility that CTD-associated RNA fragments were involved (Fig. S4). GST-DynLL1-binding was also observed for matC, while rnaC exhibited a poor interaction (Fig. 3B). Specificity of the interaction with DynLL1 was further confirmed by using the GST-fusion proteins of DynTctex1, DynTctex2, DynLL2, and DynRb1, which did not interact with the capsids (Fig. S5). Thus, we conclude that DynLL1 is the dominant if not exclusive light chain capsid-binding partner and that the strength of DynLL1 binding correlated with cytoplasmic transport. The absence of a DCC GST-DynLL1-interaction (Fig. 3B) further indicates that poor exposure of the CTD on rnaC is responsible for DynLL1 binding and cytosolic capsid transport. For verification of this hypothesis we used rnaC *in vitro* phosphorylated by protein kinase C, which enhances CTD exposure.[6] Phosphorylation in fact increased GST-DynLL1 interaction (Fig. S4) and microinjection of these capsids consistently showed a similar efficiency of transport in *Xenopus laevis* oocytes as observed for matC (Fig. S6; 20% at 15 min), suggesting that CTD exposure is essential.

To show that the capsid dynein-interactions are not different between *Xenopus laevis* oocytes and hepatocytes, we then analyzed the binding of the different capsids to DynIC of cytosolic extracts of the hepatoma cell line HuH7. This approach was chosen as perturbations upon microinjections make the analysis of active transport impossible and infections of HBV susceptible cells cannot distinguish between transport of cytosolic capsids and capsids in endosomal vesicles. Analysis of DynLL1 binding in turn could reflect the interaction with the DynLL1 fraction, which is unbound to dynein, not allowing conclusions about capsid transport. Consistent with the need of MTs and dynein shown in the previous assays, the pull-down assays confirmed that empC and matC bound (indirectly) to DynIC, while binding of rnaC was weaker and not observed for DCC (Fig. S7).

Binding of empC to DynIC requires DynLL1

As most DynLL1 interaction partners bind to dynein-unrelated DynLL1, we then investigated if empC DynLL1-interaction still allows DynLL1 to bind to DynIC. We used GST fused to the DynLL1 binding site (aa 1–295)[37] as expression of full-length DynIC failed. Considering that GST dimerizes, we removed the GST domain after factor Xa cleavage (Fig. S8). We tested heterotrimer formation by co-sedimentation, showing that DynLL1 sedimented only in the presence of the capsids (Fig. 4) and that the capsid GST-DynLL1-interactions were specific for DynLL1 domain and not caused by GST. In the presence of empC, GST-DynIC$_{1\text{-}295}$ was sedimented in the presence of DynLL1 only, supporting its function as a linker to dynein. Of note, the sediment contained only the full-length GST-DynIC$_{1\text{-}295}$ expression fragment, confirming binding specificity.

DynLL1 and DynLL2 differ in only six amino acids (Fig. S9A), which we exchanged separately by site-directed mutagenesis. Expression as GST-fusion proteins revealed a single band for each mutant after purification (Fig. S9B) and pull-down assays

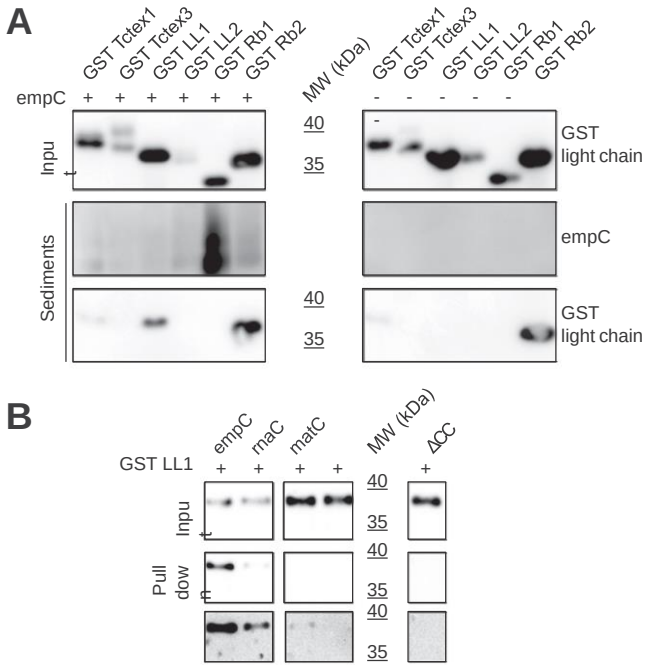

Fig. 3. Interaction of empC and matC with GST-dynein light chains. Western blots after SDS PAGE (light chains) or NAGE (empC). Light chains were detected by anti-GST antibodies and capsids by anti-capsid antibodies. (A) Co-sedimentation assays. Upper row: GST-dynein light chains in the reaction mixture, middle row: sedimented capsids, lower row: co-sedimented GST-dynein light chain proteins. All bands were obtained from two parallel gels and Western blots. (B) Pull-down assays of GST-DynLL1 using different capsids as indicated on top of the panels. Upper row: input GST-DynLL1, middle row: coprecipitated GST-DynLL1 (short exposure), lower row: long exposure. The original blots are shown in the supporting information. empC, empty capsids; DynLL1, dynein light chain LC8-type 1; GST, glutathione S-transferase; matC, mature rcDNA; NAGE, native agarose gel electrophoresis; PAGE, polyacrylamide gel electrophoresis; rnaC, RNA-containing capsids.

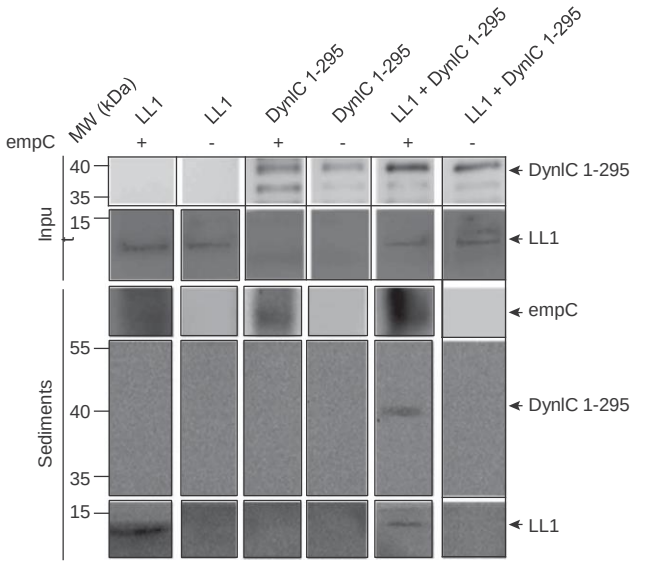

Fig. 4. Co-sedimentation of DynLL1 and DynIC 1-295 with empC. Western blot after SDS PAGE using anti-GST antibodies (GST-DynIC$_{1\text{-}295}$) or anti-DynLL1 antibodies (LL1). Capsids were detected by Western blot after NAGE. Input: proteins in the reaction mixture; sediments: capsid co-sedimented proteins. The original blots are shown in the supporting information. empC, empty capsids; DynIC, dynein intermediate chain; DynLL1, dynein light chain LC8-type 1; GST, glutathione S-transferase; matC, mature rcDNA; NAGE, native agarose gel electrophoresis; PAGE, polyacrylamide gel electrophoresis; rnaC, RNA-containing capsids.

using RRL revealed that all mutant proteins – except GST-DynLL1$_{H41Y}$ – bound DynIC (Fig. S9C). However, binding to empC was observed for all mutant proteins (Fig. S9D).

In vitro competition of the indirect empC MT-interaction by GST-DynLL1

To investigate if another linker connects capsids to dynein with regard to core protein dimers, we first used empC *in vitro* MT binding assays, adding a 100-fold excess of GST-DynLL1. As shown in Fig. 5A, the MT colocalization of empC was reduced and quantification confirmed a significant decrease (Fig. 5B). Competition of capsid binding using GST-DynLL1$_{H41Y}$, also reduced colocalization significantly (Fig. 5B), suggesting that the reduction of empC binding was not caused by interference of wild-type GST-DynLL1 with the dynein complex.

In vivo competition of DynLL1 and DynLL1$_{H41Y}$ with retrograde empC transport

To demonstrate that the binding reduction corresponds to transport inhibition, we microinjected empC with an eightfold excess of a GST-DynLL1 or GST-DynLL1$_{H41Y}$ into *Xenopus laevis* oocytes. Quantification of the capsid-associated NPCs revealed that both GST-DynLL1 and the mutant reduced the number of capsid-associated NPCs by sixfold at 15 and 60 min (Fig. 5C) and the number of capsids per NPC by 2.5-fold (Fig. 5D). Consistent with the reduction observed in *in vitro* MT capsid-binding assay, the H41Y mutant also reduced empC transport, confirming that the inhibitory effect of wild-type GST-DynLL1 was neither caused by interference with preformed dynein complexes nor that wild-type GST-DynLL1 interfered with dynein formation during the observation period.

Discussion

To date, few studies exist on cytoplasmic trafficking of HBV capsids. Lipofection studies showed that MT-depolymerization by nocodazole (Paclitaxel) abolishes initiation of replication *in cellulo* and also transport of matC to the nucleus.[5] MT-depolymerizing agents are used for treatment of different solid cancers, but their severe side effects prevent their use in HBV treatment. To find more specific targets we analyzed cytosolic capsid transport in detail. The use of different capsids allowed us to address different steps of the viral life cycle: while investigations using empC focus on cytoplasmic capsid removal, matC have significance on the infection process and cccDNA amplification. The observation that both capsids were transported to the nucleus after cytosolic microinjection in *Xenopus laevis* oocytes within 15 min, followed by a rapid increase within 45 min, suggests an active retrograde transport using dynein. This conclusion is in agreement with the need for MT and with the velocity observed for adenoviral capsids in somatic cells (3.6 μm/min[38]).

At the NE, rnaC were found less frequently and DCC were never found. These findings led to the hypothesis that CTD exposure is required, as the CTD is fixed inside the capsids' lumen in rnaC,[39] but exposed on matC[6] and PrnaC. We interpret the limited transport of rnaC as a result of a minor proportion of rnaC containing less RNA, or capsid breathing allowing tempo-

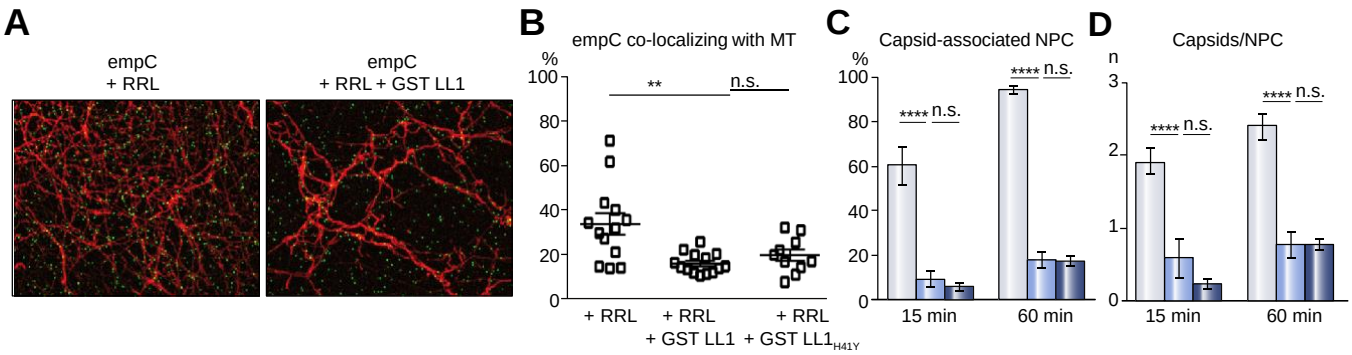

Fig. 5. Competition of empC – MT interaction by GST-DynLL1. (A) *In vitro* binding assays. Fluorescence microscopy of *in vitro* polymerized rhodamine-labeled MT (red) and empC, detected by indirect immune fluorescence (green) in the presence of RRL. Left: control without GST-DynLL1, right: in the presence an excess of GST-DynLL1. (B) Quantification of the empC – MT interaction. Quantification was based on 41 microscopical fields of six assays. Y-axis: percentage of capsids overlapping with MT. Each point shows the result of one microscopical field. (C) Percentage of empC-decorated NPCs at 15 and 60 min post injection. Light blue bars: control in the absence of GST-DynLL1, middle blue bars: after co-microinjection of GST-DynLL1, dark blue bars: after co-injection of GST-DynLL1 H41Y mutant. Quantification was done on 123 sections derived from different sites of the NE of 10 microinjected oocytes and based on 99 NPCs (15 min) and 148 NPCs (60 min) for empC without GST-DynLL1, 79 NPCs (15 min) and 88 NPCs (60 min) for empC with GST-DynLL1 and 187 NPCs (15 min) and 189 NPCs (60 min) for empC with GST-DynLL1$_{H41Y}$. (D) Average number of capsids per NPC. The bars show the standard deviations, significant differences by unpaired Student's *t* Test with unequal variances are indicated by *. empC, empty capsids; DynLL1, dynein light chain LC8-type 1; GST, glutathione S-transferase; matC, mature rcDNA; MT, microtubules; NE, nuclear envelope; NPC, nuclear pore complex; rnaC, RNA-containing capsids; RRL, rabbit reticulocyte lysate. (This figure appears in colour on the web.)

rary Cp dimer dissociation from the intact capsid,[40] enabling CTD exposure.

In vitro binding to *in vitro* polymerized MT showed the need for a soluble cytoplasmic factor, which is in line with the use of dynein, which could be confirmed in lysates from hepatoma cells. Binding along the entire length of the MT further supported this conclusion and argues against a movement via tubulin polymerization. Attachment of empC and matC to MT in the binding assays was similar, although slightly better for empC. In contrast, rnaC showed a much lower level of colocalization with MTs, which is consistent with its reduced transport rate in *Xenopus laevis* oocytes.

To search for a potential interaction partner on the dynein motor complex we used dynein light chains expressed as GST-fusion proteins. The finding that all fusion proteins interacted with DynIC from RRL demonstrated not only a proper folding of the DynIC binding groove, but also their physiological dimerization capacity. Thus, we conclude that the identification of DynLL1 as the only capsid interaction partner amongst the dynein light chains (except DynRb2) was based on a proper conformation. Our results on capsid binding correspond to the transport capacity of the different capsids in that it was very low for rnaC even upon prolonged exposure time of the Western blot. In agreement with this correlation, we did not observe any DynLL1 interaction with DCC.

Acting as a linker to the dynein complex, DynLL1 needs simultaneous binding to DynIC and capsids. This was confirmed by co-sedimentation of the multimeric DynIC-DynLL1-capsid-complex. This assay requires high capsid amounts and was thus restricted to empC.

Strikingly, no binding was observed for DynLL2. Mutating the six amino acids differing between DynLL1 and DynLL2 showed that the DynLL1 H41Y mutant failed to bind DynICs. All mutants bound empC (Fig. S9A), allowing us to use GST-DynLL1 H41Y as a control, which cannot interfere with the dynein complex.

To exclude the role of DynLL1-independent pathways, we demonstrated that an excess of GST-DynLL1 reduced empC MT colocalization to a level similar to that observed for rnaC, leading to the conclusion that DynLL1 is at least the major binding partner linking the capsids to MT via dynein. This presumption was confirmed by the co-microinjection experiments of empC with GST-DynLL1, showing a reduction of empC transport to the level of rnaC transport (13% *vs.* 14%). As the co-injections of GST-DynLL1$_{H41Y}$ yielded the same reduction, we further conclude that inhibition by GST-DynLL1 was not caused by formation of non-functional dynein due to GST-DynLL1 incorporation into dynein.

In summary, our study identified DynLL1 as a functional binding partner for matC and empC. We identified the outer surface of this 89 aa-long protein, as a binding region, which does not interfere with its function in the dynein motor complex. Thus, we conclude that targeting this domain could be a possible drug target for hepatitis B and that the comparison of wild-type DynLL1 and DynLL1 H41Y mutant structures will further help in rational drug design.

Numerous interaction partners have been described for the different dynein chains but evidence for their implication in transport is frequently lacking. It has been functionally verified is that roadblock is involved in the transport of Rab 6 for vesicle transport[41] and Tctex1 is needed for transport of the small GTPase RagA.[42]

While most of the dynein chains exist only in association with the dynein motor complex, a significant part of DynLL1 is not dynein-associated.[32] Thus, several proteins *e.g.* Bim,[43] occupy the same binding grooves required for DynIC binding. Viral DynLL1 binding partners were also reported, as *e.g.* the foamy virus capsid protein, gag, which colocalizes with DynLL1 at the MTOC.[44] As DynLL1 also binds to the MTOC via the centrosomal protein CDK5RAP2,[45] no conclusion regarding the implication of this viral-DynLL1 binding on transport can be deduced. Another example is the bovine immunodeficiency virus, which interacts with DynLL1 and which needs retrograde transport via MT for infection. Overexpression of dynamitin, which dissociates the dynein-bound dynactin complex from dynein, reduces viral infection,[46] indicating that in fact dynactin is, in fact, the functional interaction partner. As reviewed by Barbar[47] only the dynein interaction with Dazl, which is required for MT-dependent mRNA localization in male germ cell development in mammals, was proven to be DynLL1-dependent.[34] Thus, we conclude that our data for the functional

need of DynLL1-binding for HBV capsid transport is the first evidence of a viral cargo.

Financial support

We thank the Fondation pour la recherche médicale (FRM; www.frm.org; équipe FRM 2011 DEQ20110421299) and the National French Agency for Research against HIV and Hepatitis Viruses (ANRS; http://www.anrs.fr/; AAP 2010-2, AAP 2013-2), which supported the work with the salary of QO and consumables for MK, the Centre National de la recherche scientifique (CNRS; www.cnrs.fr; PICS 05864) and the Agence française pour la promotion de l'enseignement supérieur (http://www.campusfrance.org; PHC OSMOSE 2012), which supported the collaboration between the authors by travel grants given to MK, the Natural Sciences and Engineering Research Council of Canada (NSERC; www.nserc-crsng.gc.ca), which supported the group in Vancouver with two grants to NP (RGPAS 412254-11, RGPIN 227926-11). The funders had no role in study design, data collection and analysis, decision to publish, or preparation of the manuscript.

Conflict of interest

The authors declare no conflicts of interest that pertain to this work.

Please refer to the accompanying ICMJE disclosure forms for further details.

Authors' contributions

SA and NP performed the electron microscopy; QO, LG, CC, EB, AC, DB, JR, CA, BR, MLB and FA performed the other experiments, IS and AD produced and characterized the *E. coli* capsids, MK coordinated the research, QO and MK analyzed data and wrote the manuscript.

Acknowledgements

We thank Beate Sodeik, MH Hannover, Germany, for the GST-dynein chain expression plasmids. We also thank Bradford Ross of the BioImaging Facility at the University of British Columbia for help with electron tomography. We further thank Harald Wodrich, Bordeaux, for critical reading of the manuscript and the Bordeaux Imaging Centre (BIC) for using their microscope facility.

Supplementary data

Supplementary data associated with this article can be found, in the online version, at https://doi.org/10.1016/j.jhep.2017.10.032.

References

1 World Health Organization. Hepatitis B, Fact sheet 204; 2017.

2 Blondot M-L, Bruss V, Kann M. Intracellular transport and egress of hepatitis B virus. J Hepatol 2016;64:S49–S59. https://doi.org/10.1016/j.jhep.2016.02.008.

3 Yan H, Zhong G, Xu G, He W, Jing Z, Gao Z, et al. Sodium taurocholate cotransporting polypeptide is a functional receptor for human hepatitis B and D virus. Elife 2012;1:1–28. https://doi.org/10.7554/eLife.00049.

4 Schulze A, Gripon P, Urban S. Hepatitis B virus infection initiates with a large surface protein-dependent binding to heparan sulfate proteoglycans. Hepatology 2007;46:1759–1768. https://doi.org/10.1002/hep.21896.

5 Rabe B, Glebe D, Kann M. Lipid-mediated introduction of hepatitis B virus capsids into nonsusceptible cells allows highly efficient replication and facilitates the study of early infection events. J Virol 2006;80:5465–5473. https://doi.org/10.1128/JVI.02303-05.

6 Rabe B, Vlachou A, Panté N, Helenius A, Kann M. Nuclear import of hepatitis B virus capsids and release of the viral genome. Proc Natl Acad Sci U S A 2003;100:9849–9854.

7 Gallucci L, Kann M. Nuclear import of hepatitis B virus capsids and genome. Viruses 2017;9. https://doi.org/10.3390/v9010021.

8 Königer C, Wingert I, Marsmann M, Rösler C, Beck J, Nassal M. Involvement of the host DNA-repair enzyme TDP2 in formation of the covalently closed circular DNA persistence reservoir of hepatitis B viruses. Proc Natl Acad Sci U S A 2014;111:E4244–E4253. https://doi.org/10.1073/pnas.1409986111.

9 Qi Y, Gao Z, Xu G, Peng B, Liu C, Yan H, et al. DNA polymerase j is a key cellular factor for the formation of covalently closed circular DNA of Hepatitis B virus. PLoS Pathog 2016;12:e1005893. https://doi.org/10.1371/journal.ppat.1005893.

10 Quasdorff M, Protzer U. Control of hepatitis B virus at the level of transcription. J Viral Hepat 2010;17:527–536. https://doi.org/10.1111/j.1365-2893.2010.01315.x.

11 Seeger C, Mason WS. Hepatitis B virus biology. Microbiol Mol Biol Rev 2000;64:51–68.

12 Gerelsaikhan T, Tavis JE, Bruss V. Hepatitis B virus nucleocapsid envelopment does not occur without genomic DNA synthesis. J Virol 1996;70:4269–4274.

13 Wang J, Shen T, Huang X, Kumar GR, Chen X, Zeng Z, et al. Serum hepatitis B virus RNA is encapsidated pregenome RNA that may be associated with persistence of viral infection and rebound. J Hepatol 2016;65:700–710. https://doi.org/10.1016/j.jhep.2016.05.029.

14 Ning X, Nguyen D, Mentzer L, Adams C, Lee H, Ashley R, et al. Secretion of genome-free hepatitis B virus–single strand blocking model for virion morphogenesis of para-retrovirus. PLoS Pathog 2011;7:e1002255. https://doi.org/10.1371/journal.ppat.1002255.

15 Chen C, Wang JC-Y, Pierson EE, Keifer DZ, Delaleau M, Gallucci L, et al. Importin b can bind hepatitis B virus core protein and empty core-like particles and induce structural changes. PLoS Pathog 2016;12:e1005802. https://doi.org/10.1371/journal.ppat.1005802.

16 Kann M, Sodeik B, Vlachou A, Gerlich WH, Helenius A. Phosphorylation-dependent binding of hepatitis B virus core particles to the nuclear pore complex. J Cell Biol 1999;145:45–55.

17 Bertoletti A, Ferrari C, Fiaccadori F, Penna A, Margolskee R, Schlicht HJ, et al. HLA class I-restricted human cytotoxic T cells recognize endogenously synthesized hepatitis B virus nucleocapsid antigen. Proc Natl Acad Sci U S A 1991;88:10445–10449.

18 Deres K, Schroder CH, Paessens A, Goldmann S, Hacker HJ, Weber O, et al. Inhibition of hepatitis B virus replication by drug-induced depletion of nucleocapsids. Science 2003;299:893–896.

19 Chu CM, Yeh CT, Chien RN, Sheen IS, Liaw YF. The degrees of hepatocyte nuclear but not cytoplasmic expression of hepatitis B core antigen reflect the level of viral replication in chronic hepatitis B virus infection. J Clin Microbiol 1997;35:102–105.

20 Kim TH, Cho EY, Oh HJ, Choi CS, Kim JW, Moon HB, et al. The degrees of hepatocyte cytoplasmic expression of hepatitis B core antigen correlate with histologic activity of liver disease in the young patients with chronic hepatitis B infection. J Korean Med Sci 2006;21:279–283. https://doi.org/10.3346/jkms.2006.21.2.279.

21 Moraleda G, Saputelli J, Aldrich CE, Averett D, Condreay L, Mason WS. Lack of effect of antiviral therapy in nondividing hepatocyte cultures on the closed circular DNA of woodchuck hepatitis virus. J Virol 1997;71:9392–9399.

22 Marcellin P, Lau GKK, Bonino F, Farci P, Hadziyannis S, Jin R, et al. Peginterferon alfa-2a alone, lamivudine alone, and the two in combination in patients with HBeAg-negative chronic hepatitis B. N Engl J Med 2004;351:1206–1217. https://doi.org/10.1056/NEJMoa040431.

23 Wang X-Y, Chen H-S. Emerging antivirals for the treatment of hepatitis B. World J Gastroenterol 2014;20:7707–7717. https://doi.org/10.3748/wjg.v20.i24.7707.

24 Cui X, Ludgate L, Ning X, Hu J. Maturation-associated destabilization of hepatitis B virus nucleocapsid. J Virol 2013;87:11494–11503. https://doi.org/10.1128/JVI.01912-13.

25 Luby-Phelps K. Physical properties of cytoplasm. Curent Opin Cell Biol 1994;6:3–9.

26 Luby-Phelps K. Cytoarchitecture and physical properties of cytoplasm: volume, viscosity, diffusion, intracellular surface area. Int Rev Cytol 2000;192:189–221.

27 Erickson HP. Evolution of the cytoskeleton. BioEssays 2007;29:668–677. https://doi.org/10.1002/bies.20601.

28 Zhai Y, Kronebusch PJ, Simon PM, Borisy GG. Microtubule dynamics at the G2/M transition: abrupt breakdown of cytoplasmic microtubules at nuclear envelope breakdown and implications for spindle morphogenesis. J Cell Biol 1996;135:201–214.

29 Galbraith JA, Reese TS, Schlief ML, Gallant PE. Slow transport of unpolymerized tubulin and polymerized neurofilament in the squid giant axon. Proc Natl Acad Sci U S A 1999;96:11589–11594.

30 Pavin N, Tolic´-Nørrelykke IM. Dynein, microtubule and cargo: a ménage à trois. Biochem Soc Trans 2013;41:1731–1735. https://doi.org/10.1042/BST20130235.

31 Pfister KK, Shah PR, Hummerich H, Russ A, Cotton J, Annuar AA, et al. Genetic analysis of the cytoplasmic dynein subunit families. PLoS Genet 2006;2:e1. https://doi.org/10.1371/journal.pgen.0020001.

32 King SM, Barbarese E, Dillman JF, Patel-King RS, Carson JH, Pfister KK. Brain cytoplasmic and flagellar outer arm dyneins share a highly conserved Mr 8.000 light chain. J Biol Chem 1996;271:19358–19366.

33 Rapali P, Szenes Á, Radnai L, Bakos A, Pál G, Nyitray L. DYNLL/LC8: a light chain subunit of the dynein motor complex and beyond. FEBS J 2011;278:2980–2996. https://doi.org/10.1111/j.1742-4658.2011.08254.x.

34 Lee KH, Lee S, Kim B, Chang S, Kim SW, Paick J-S, et al. Dazl can bind to dynein motor complex and may play a role in transport of specific mRNAs. EMBO J 2006;25:4263–4270. https://doi.org/10.1038/sj.emboj.7601304.

35 Crowther RA, Kiselev NA, Bottcher B, Berriman JA, Borisova GP, Ose V, et al. Three-dimensional structure of hepatitis B virus core particles determined by electron cryomicroscopy. Cell 1994;77:943–950.

36 Wang JC-Y, Nickens DG, Lentz TB, Loeb DD, Zlotnick A. Encapsidated hepatitis B virus reverse transcriptase is poised on an ordered RNA lattice. Proc Natl Acad Sci U S A 2014;111:11329–11334. https://doi.org/10.1073/pnas.1321424111.

37 Nyarko A, Barbar E. Light chain-dependent self-association of dynein intermediate chain. J Biol Chem 2011;286:1556–1566. https://doi.org/10.1074/jbc.M110.171686.

38 Bremner KH, Scherer J, Yi J, Vershinin M, Gross SP, Vallee RB. Adenovirus transport via direct interaction of cytoplasmic dynein with the viral capsid hexon subunit. Cell Host Microbe 2009;6:523–535. https://doi.org/10.1016/j.chom.2009.11.006.

39 Wang JC-Y, Dhason MS, Zlotnick A. Structural organization of pregenomic RNA and the carboxy-terminal domain of the capsid protein of hepatitis B virus. PLoS Pathog 2012;8:e1002919. https://doi.org/10.1371/journal.ppat.1002919.

40 Ceres P, Zlotnick A. Weak protein-protein interactions are sufficient to drive assembly of hepatitis B virus capsids. Biochemistry 2002;41:11525–11531. https://doi.org/10.1021/bi0261645.

41 Wanschers B, van de Vorstenbosch R, Wijers M, Wieringa B, King SM, Fransen J. Rab6 family proteins interact with the dynein light chain protein DYNLRB1. Cell Motil Cytoskeleton 2008;65:183–196. https://doi.org/10.1002/cm.20254.

42 Merino-Gracia J, García-Mayoral MF, Rapali P, Valero RA, Bruix M, Rodríguez-Crespo I. DYNLT (Tctex-1) forms a tripartite complex with dynein intermediate chain and RagA, hence linking this small GTPase to the dynein motor. FEBS J 2015;282:3945–3958. https://doi.org/10.1111/febs.13388.

43 Day CL, Puthalakath H, Skea G, Strasser A, Barsukov I, Lian L, et al. Localization of dynein light chains 1 and 2 and their pro-apoptotic ligands. Biochem J 2004;377:597–605. https://doi.org/10.1042/BJ20031251.

44 Petit C, Giron M-L, Tobaly-Tapiero J, Bittoun P, Real E, Jacob Y, et al. Targeting of incoming retroviral Gag to the centrosome involves a direct interaction with the dynein light chain 8. J Cell Sci 2003;116:3433–3442. https://doi.org/10.1242/jcs.00613.

45 Jia Y, Fong K-W, Choi Y-K, See S-S, Qi RZ. Dynamic recruitment of CDK5RAP2 to centrosomes requires its association with dynein. PLoS ONE 2013;8:e68523. https://doi.org/10.1371/journal.pone.0068523.

46 Su Y, Qiao W, Guo T, Tan J, Li Z, Chen Y, et al. Microtubule-dependent retrograde transport of bovine immunodeficiency virus. Cell Microbiol 2010;12:1098–1107. https://doi.org/10.1111/j.1462-5822.2010.01453.x.

47 Barbar E. Dynein light chain LC8 is a dimerization hub essential in diverse protein networks. Biochemistry 2008;47:503–508. https://doi.org/10.1021/bi701995m.